Optimized Corrugated Tapered Slot Antenna for mm-Wave Applications

Claudio Jarufe, Rafael Rodriguez, Valeria Tapia, Pablo Astudillo, David Monasterio, Rocio Molina, F. P. Mena, Nicolas Reyes, and Leonardo Bronfman

***Abstract*— We present a novel approach to design a high-performance tapered slot antenna (TSA) at millimeter-wave frequencies. Commonly, TSAs are designed using profiles expressed as simple functions (linear, exponential, Fermi, or constant width). Some improvement can be achieved by the use of corrugations of fixed dimensions. This usual approach, however, gives little room for improvement in their performance. To overcome this situation, we have developed a new approach: the use of a nonspecific profile and variable corrugations along the antenna, both of which can be optimized to considerably improve its performance. For the optimization, we have used a particle-swarm algorithm allowing us to achieve an excellent performance in the entire W-band. To demonstrate the efficiency of this new approach, we have implemented an optimized antenna using standard printed circuit board (PCB)-prototyping methods. Across the whole W-band, the constructed antenna shows sidelobe levels, reflection coefficient, and cross polarization below −16, −10, and −25 dB, respectively. These results are in good agreement with simulations which also predict possible operation down to 60 GHz. Finally, given its small footprint and the fact that it has been fed by a microstrip line, this antenna can be used in compact electronics providing excellent performance such as that required in radio astronomy or telecommunications.**

***Index Terms*— Active antennas, antenna arrays, microwave antennas, particle-swarm optimization (PSO), slot antennas.**

I. Introduction

In 1979 Gibson [1] introduced the "Vivaldi aerial," a planar antenna capable of producing a symmetrical endfire radiation pattern. Several studies have introduced variations to the original design to increase their performance [2], [3]. These antennas have been extensively studied at frequencies below 15 GHz because they present several advantages:

1) broad bandwidth;
2) narrow beam widths (down to 15° at −3 dB);
3) symmetrical radiation patterns;
4) greater compactness than horn antennas;
5) easier integration with integrated circuits.

These characteristics make them very interesting for applications such as satellite communications, radio telescopes, and millimeter-wave (mm-wave) imaging systems [4], [5]. In these applications, there is an increasing interest in high-density multibeam systems, and it is in this topic where tapered slot antenna (TSA) arrays with integrated technology could be very useful.

At mm-wave frequencies and above, the usual antenna element is a horn antenna and the connection with the rest of the circuit is usually achieved using waveguides and planar transmission lines. These characteristics limit compaction and further integration with integrated circuits. In certain applications, a TSA could be more suitable. However, a few studies have been carried out at millimeter wavelengths, since their construction is more complicated due to the need for thin substrates with low dielectric constant. Some efforts to construct a TSA that covers the W-band have been carried out, but with limited success. Table I summarizes these efforts and presents a comparison of the beam properties and their manufacturing process. In [6], a TSA built with a surface micromachined process was measured, but the E-plane was found to be asymmetric due to the slot line feed. The TSA measured in [7] was manufactured in a simpler way (Laser PCB Prototyping), but the simulated E- and H-planes were asymmetrical respect to their maximums. The Vivaldi antenna presented in [8] was built in low temperature cofired ceramic (LTCC) showing good properties but operates in a reduced bandwidth. In all the aforementioned work and that reported in other frequency bands, the antennas are constructed with well-known profiles (linear, constant width, exponential, and Fermi) and the depth of the corrugations along the antenna is fixed, but there is no further analysis on new profiles or variable corrugations. Other works presenting only simulations or measurements of reflections (S_{11}) alone are not discussed here.

In this paper, we present the design and implementation of a TSA with an optimized generic profile and variable corrugations to reduce cross polar radiation and sidelobes over a large bandwidth (approximately 40% of fractional bandwidth). Importantly, the shape and number of corrugations were also included in the optimization process. To increase the efficiency of the optimization algorithm and to avoid local minima problems, a particle-swarm optimization (PSO) method was used. The result is an antenna with excellent properties across the entire W-band. Sidelobe levels (SLs), reflection coefficient,

Manuscript received February 13, 2017; revised August 19, 2017; accepted October 18, 2017. Date of publication January 24, 2018; date of current version March 1, 2018. This work was supported in part by the Quimal-CONICYT Fund under Project N 140002, in part by Fondecyt under Grant 1151022, in part by ESO-Chile Joint Committee for Development of Astronomy, and in part by the Center of Excellence in Astrophysics and Associated Technologies under Grant PBF 06.

C. Jarufe, R. Rodriguez, V. Tapia, P. Astudillo, D. Monasterio, R. Molina, F. P. Mena, and N. Reyes are part of the Electrical Engineering Department, Universidad de Chile, Santiago 7591245, Chile.

L. Bronfman is part of the Astronomy Department, Universidad de Chile, Santiago 7591245, Chile.

Color versions of one or more of the figures in this paper are available online at http://ieeexplore.ieee.org.

Digital Object Identifier 10.1109/TAP.2018.2797534

TABLE I
COMPARISON OF W-BAND TSAs

Ref.	Profile	Corrugations	Manufacture Tech.	Bandwidth GHz	Sidelobe level dB	Cross Pol. level dB	S11 dB
[6]	Exponential	Constant	SM [a]	65-115	−8	N.A.	−9
[7]	Exponential	No	LPKF [b]	75-110	−10	N.A.	−7
[8]	Exponential	Constant	LTCC [c]	75-82	−8	N.A.	−15
This work	Optimized	Optimized	LPKF	75-110	−16	−25	−10

[a] Surface micromachining.
[b] Laser prototyping.
[c] Low Temperature Cofired Ceramic.

and cross polarization are below −16, −10, and −25 dB, respectively. Moreover, the measured patterns in the E- and H-planes show very good symmetry with respect to their maximum. It is also important to note that the simulations predict the possibility of extending the frequency coverage of the antenna down to approximately 60 GHz.

II. DESIGN

The design of the TSA was performed using a custom-made optimization program and HFSS [9]. The design process was divided into two stages. First, only the radiating part was simulated and optimized. Symmetries in the electromagnetic (EM) field were used whenever possible in order to reduce computation times. In the second stage, a microstrip-to-slot-line transition was included in the simulation.

A. Antenna Design

The TSA is a class of endfire traveling-wave antenna known as surface-wave antenna. It consists of a tapered slot which has been etched within the metallic surface on a dielectric substrate. The E-plane is parallel to the substrate since the field is attached to the horizontally separated tapers prior to being radiated along the direction of the substrate. The EM wave moves through the metal tapers until a separation of about half a wavelength has been reached [2]. At this point, the EM wave uncouples from the metallic taper and the antenna structure radiates into free space from the substrate end.

In order for the TSA to radiate properly, it has to behave as a surface-wave antenna. To achieve this, the effective dielectric thickness $t_{\text{eff}} = (\sqrt{\epsilon_r} - 1)t$ (t being the actual substrate thickness) must meet the following requirement [4]:

$$0.005\lambda_0 < t_{\text{eff}} < 0.03\lambda_0 \tag{1}$$

where λ_0 is the free space wavelength at the center frequency. For substrates with thinner effective thickness, the beamwidth will be wider, while for thicker substrates, the main beam will break up producing asymmetric beams [4]. Due to the condition stated in (1), a TSA at millimeter wavelengths has to be built in a very thin substrate with low dielectric constant. The selected substrate for the present design was Rogers Duroid 5880 ($\epsilon_r = 2.2$, $\tan\delta = 0.0009$) with a thickness of 127 μm.

Since the profile defines the radiation pattern of the TSA, an initial design was selected by dividing the antenna into

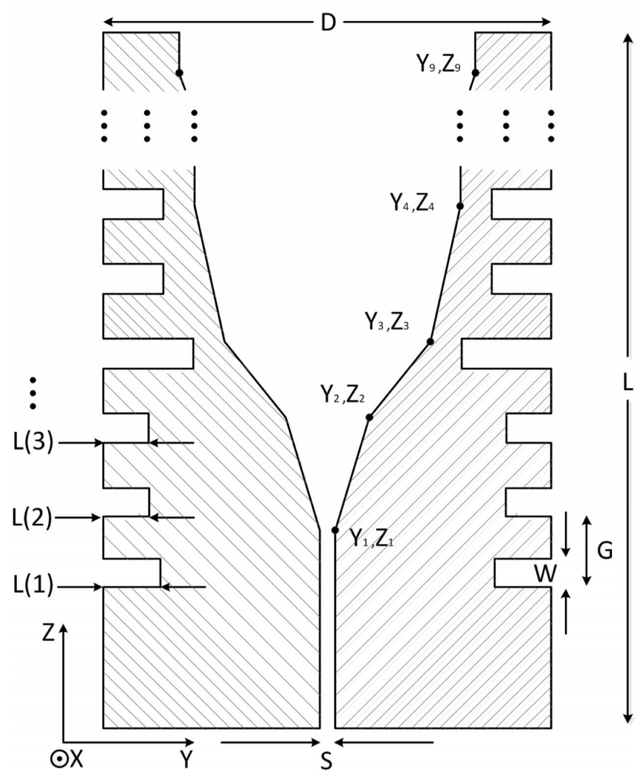

Fig. 1. Geometry of the 10-segment corrugated TSA. During the optimization, the total length L, slot width S, aperture of the antenna, number of segments of the profile, and number of corrugations were fixed.

10 linear segments. Then, corrugations were added to reduce SLs [10] and cross polarization. The geometry of the proposed radiating part of the design is shown in Fig. 1. The length of the antenna (L) was fixed to 19 mm (about 5.75 λ at 90 GHz) to produce a half-power-bandwidth of approximately 23°, according to [2]. To ensure radiation down to 60 GHz, the aperture of the antenna was fixed at 6 mm.

One of the main difficulties in building a high-frequency TSA is obtaining low input impedance. The antenna input impedance is defined by the slot line separation (S). Small values enable an impedance closer to 50 Ω. A comfortable construction value of $S = 75$ μm was selected which corresponds to an impedance of 146 Ω.

The rest of the tunable parameters are the start position of nine segments (Y and Z coordinates), the total width of the

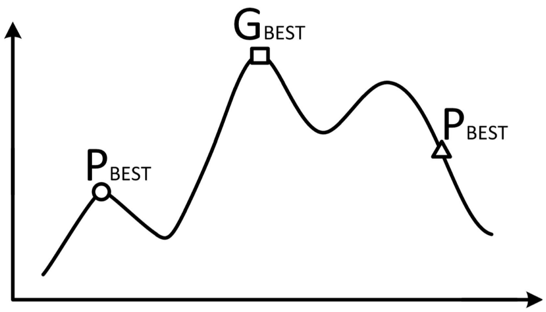

Fig. 2. Graphical 1-D representation of the PSO Algorithm. Three particles move in the solution space searching for the maximum of a function with some velocities. Each one of the particles keeps track of its own best value (p_{best}) of the objective function and the best value of the group of particles (g_{best}). The velocities of the particles are updated according to the relative positions of p_{best} and g_{best}.

antenna (D), the length of each of the 40 corrugations, and the fixed corrugation width and separation. The total number of variables is 61.

1) Particle Swarm Optimization: The variables presented above were optimized to reduce return loss, sidelobes, and cross polarization below −18 dB and to also obtain a symmetric circular beam.

The optimization was carried out using PSO [11] due to the high dimensionality and discontinuity of the problem. Under these conditions, PSO yields fast convergence, simplicity, and effectiveness [12]. Furthermore, in some cases, PSO can outperform other methods of optimization such as genetic algorithms [13]. A graphical representation of the algorithm can be seen in Fig. 2.

The values of the variables are limited such that they have physical meaning and do not unnecessarily increase the number of iterations to achieve the optimum. The restrictions added to the optimization problem were as follows.

1) Corrugations need to be small enough not to break the TSA conductor in two.
2) The added length of all the segments (in the radiation direction) must be equal to the total length of the antenna.
3) The Y_i coordinate of the segments must always be bigger than the previous Y_j coordinate to ensure the aperture increases as the wave gets radiated.
4) An absorbing wall condition was used when a variable reaches the boundary of the solution space [12].

2) Antenna Optimization Using PSO: The EM simulation was performed with HFSS and the optimization using MATLAB. A flow diagram of the optimization process is presented in Fig. 3. This method can be of great help to minimize computational resources since each EM simulation only takes a few minutes. Once one simulation is finished, HFSS is closed and MATLAB manages the simulation data. HFSS simulates the far-field pattern and return loss of the antenna at 80, 90, 100, and 110 GHz. For each frequency, the following values are exported:

1) reflections (S_{11});
2) sidelobe level (SL);

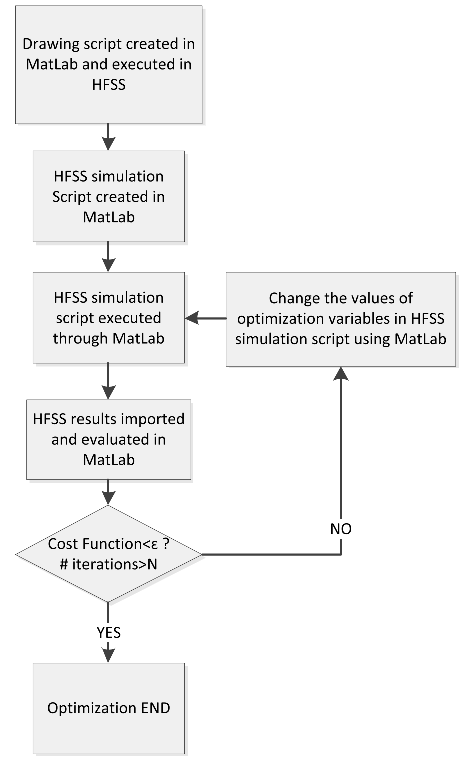

Fig. 3. Flow diagram used to implement HFSS simulations optimized with PSO. An extra condition in the number of iterations was added to stop the algorithm.

3) maximum cross polarization between ±100° (X_{pol});
4) standard deviation of the difference of the full width between half-maximum between H- and E-planes (STD_{FWHM}).

It is desired that the designed antenna has cross polarization, sidelobes, and reflections below −18 dB. In order to have a circular beam, the standard deviation between the full-width at half-maximum (FWHM) at E- and H-planes should be smaller than 0.01°. Nonlinear weights, $W(i)$, were added to set the weight to zero when the quantity is below the target value. At each frequency point, f, the cost function is defined by

$$\begin{aligned}\text{Cost}(f) = {} & W(1)\big(S_{11}(f) - S_{11}^{\text{target}}\big)^2 \\ & + W(2)\big(X_{\text{pol}}(f) - X_{\text{pol}}^{\text{target}}\big)^2 \\ & + W(3)\big(\text{SL}(f) - \text{SL}^{\text{target}}\big)^2 \\ & + W(4)\big(\text{STD}_{\text{FWHM}}(f) - \text{STD}_{\text{FWHM}}^{\text{target}}\big)^2. \quad (2)\end{aligned}$$

Finally, the objective function to minimize, using the PSO algorithm, is

$$F_{\text{obj}} = \sum_f \text{Cost}(f). \quad (3)$$

After approximately 20 days of continuous simulation using a standard workstation with 16 GB of RAM and a 3 GHz processor, and due to no further reduction in the cost function, the optimization was stopped. In total, 130 generations were simulated with 30 iterations per generation giving a total

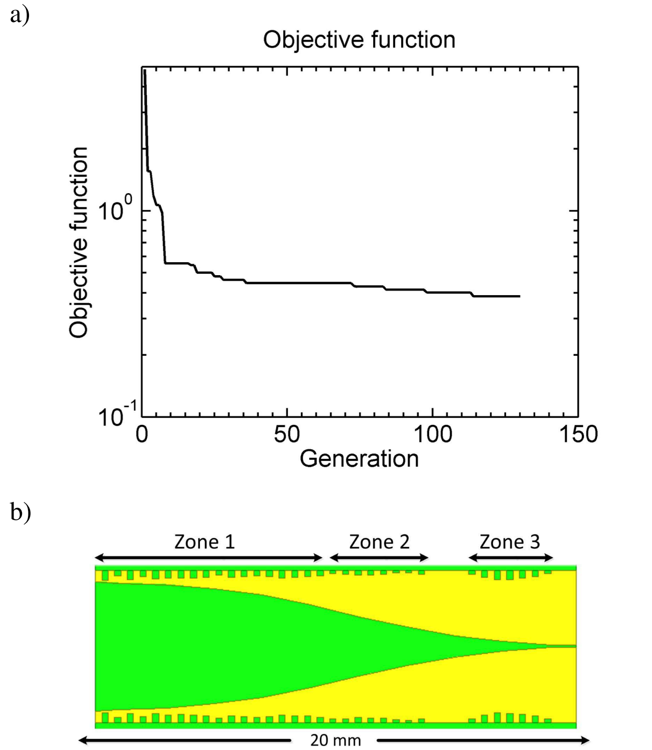

Fig. 4. (a) Minimum cost value for each generation. (b) Final design of the corrugated 10-segment TSA design (drawn to scale).

TABLE II
CORRUGATION EFFECT

Zones with corrugations	Sidelobe [dB]	Cross Pol. [dB]	S_{11} [dB]
None	−12.1	−17.0	−12.5
1	−17.2	−22.9	−13.1
3	−12.6	−16.1	−12.9
1 & 3	−18.6	−25.7	−14.9
1 & 2	−17.9	−21.0	−13.0
1 & 2 & 3	−18.9	−25.0	−15.2

of 3900 iterations. The minimization of the cost function after each generation and the optimized design can be seen in Fig. 4.

The optimization of a nonspecific profile and the corrugations allow to combine several characteristics that improve the overall performance of the antenna. Regarding the profile, the optimized TSA presented here has three distinctive sections. A small launch angle to obtain a directive beam [4] resembling a small angle linear TSA (LTSA), an intermediate shape similar to a Fermi or Vivaldi that reduces sidelobes [14], and a linear feed to obtain a frequency-independent impedance [2].

Three corrugated sections can also be distinguished in the final TSA [Fig. 4(b)]. To investigate their effect quantitatively, we performed simulations where they are not included. Table II presents the maximum sidelobe, cross polar level, and return losses when different corrugated sections are added or taken out from the final profile. In zone 1, near the radiating part, an electric field is established between the

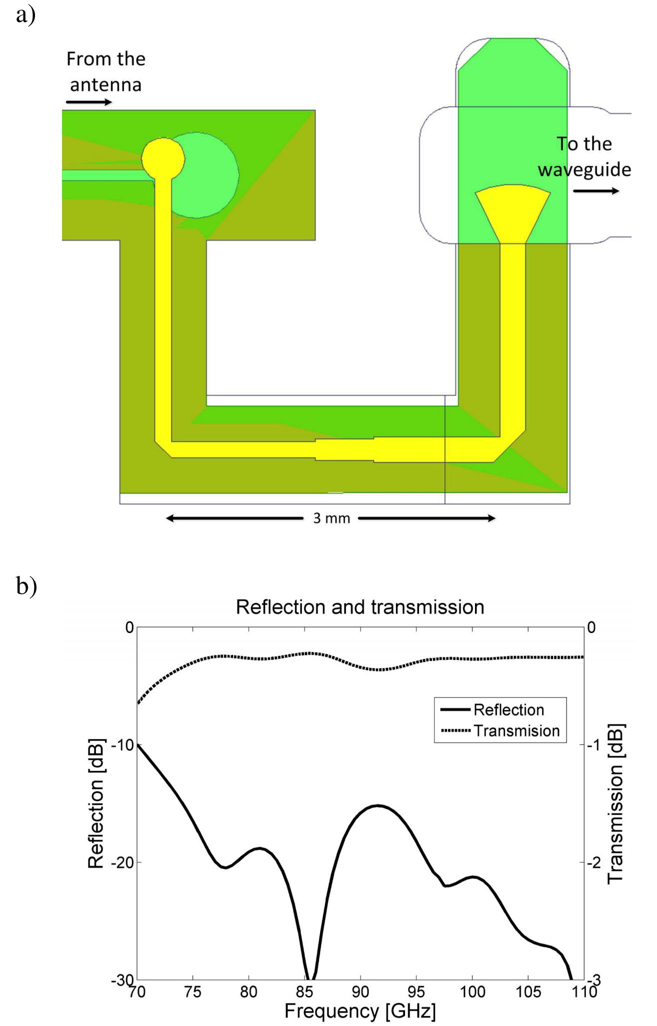

Fig. 5. (a) Design of the transition from slot line to waveguide (drawn to scale). (b) Simulated reflection and transmission of the full transition.

corrugations at the edges of the antenna [10]. The electric field inside the corrugations is parallel to the radiation direction and the magnetic field is perpendicular to the electric field. Similar to the effect of corrugations in aperture antennas [15], this field distribution affects the boundary condition of the tangential electric and magnetic fields at the edge of the antenna. Without corrugations, the electric field in the edge of the antennas is opposite to the electric field inside the aperture. With corrugations, the electric field at the edges is in the same direction as the electric field in the aperture resulting in a radiation pattern with low cross polarization and sidelobes, and allowing a better matching of the TSA to the free space. This effect is induced by the electric field inside the corrugations whose intensity becomes stronger when the length of the corrugations is less than $0.15\lambda_0$ and greater than $0.04\lambda_0$ [10]. In the optimized TSA presented here, the mean length of the corrugations in the zone 1 is 0.31 mm $\approx 0.1\lambda_0$.

In zone 2, there are almost no corrugations and the effect of adding them in this section is almost negligible. Finally, zone 3 serves to match the impedance of the slot line input to the radiating section of the TSA. These corrugations have a second-order effect on the shape of the beam. By adding

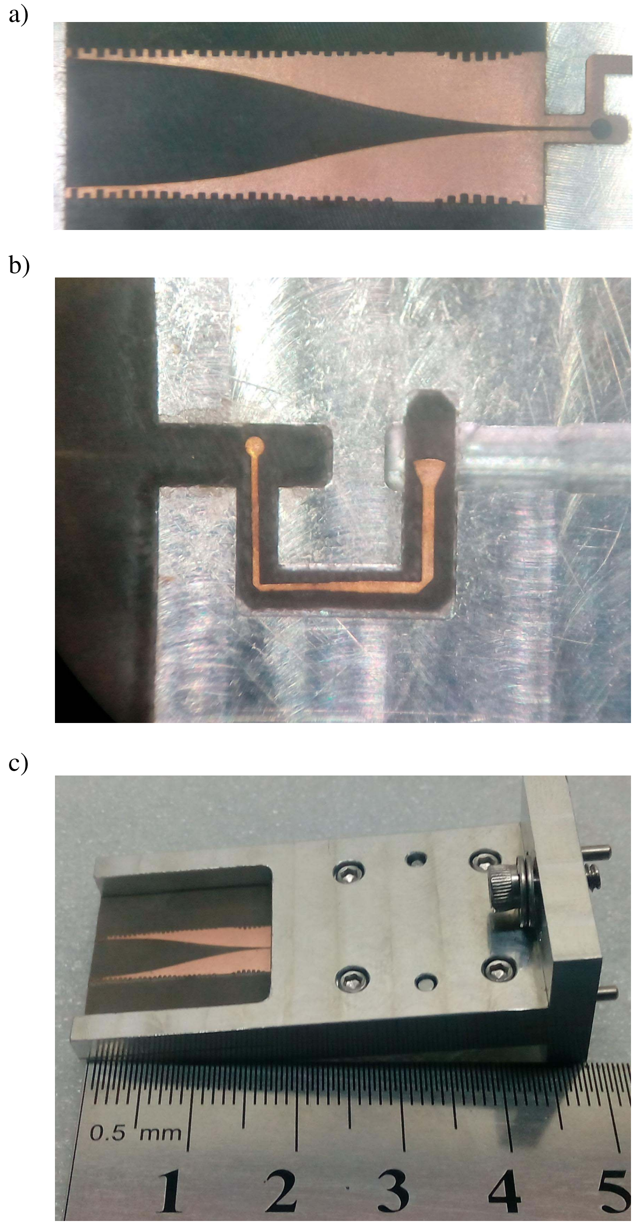

Fig. 6. Constructed TSA. (a) Bottom side of the substrate. (b) Transition from the antenna to the waveguide. It was mounted in the bottom block inside a groove to ensure proper alignment. (c) Complete block with the mounted antenna.

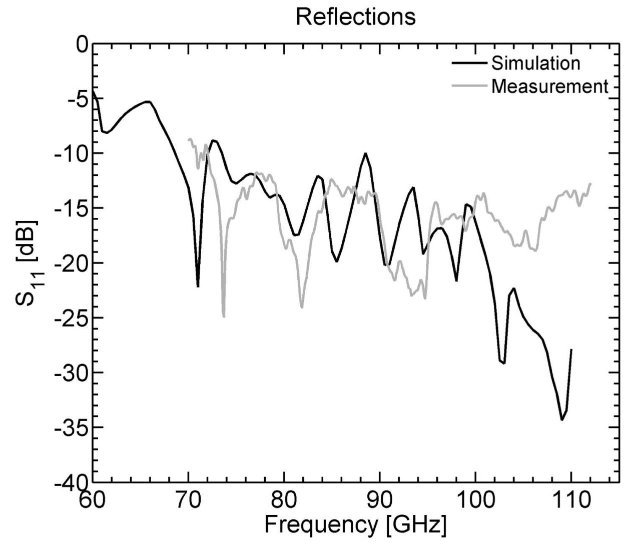

Fig. 7. Antenna reflection measurement (gray solid) and simulations (black solid). A small standing wave can be noticed in the measurement.

only corrugations in zone 1, the beam characteristics improve substantially but only when the corrugations in zone 3 are added, the reflections are diminished.

B. Transition From Slot Line to Waveguide

The beam-pattern measurement setup, as described in Section III, has a waveguide feed to test antennas. Therefore, the TSA was designed to be mounted in a metallic split block containing a rectangular waveguide. Although the antenna could have been tested using a direct transition from slot line to waveguide [16], for active-antenna applications with monolithic microwave integrated circuit integration, a transition from slot line to either microstrip or coplanar lines is preferred. For the purpose of this paper, we have selected the former transition, previous to launch the signal into the waveguide. This transition is based on the design presented in [17], where nonplanar transitions with different stub configurations are analyzed. The transition was designed using a slot line with the same width that the input slot line has in the corrugated 10-segment antenna. The microstrip-line impedance was selected to be 109 Ω.

In order to launch the signal into the waveguide, a transition from a 50 Ω microstrip line to a rectangular waveguide was designed, based on the work of [18]. This transition has return losses better than 20 dB in the W-band. The final element of the full transition is a matching line that connects the 109 and 50 Ω lines. In order to have the TSA aligned with the waveguide, two mitered microstrip bends were added to the line. The full transition, as described above, was designed to be placed over the same substrate where the antenna was constructed. Furthermore, this transition was also designed to be enclosed in a metallic cavity to avoid that its radiation affects the radiation pattern of the antenna. We were particularly careful in selecting the size of the cavity such that the cutoff frequency of waveguide modes inside them is above 120 GHz. The final design and simulations of its reflection and transmission are presented in Fig. 5. The full transition has return losses better than 15 dB.

C. Clamping of the Antenna

Due to the flexibility of the substrate and its length, the TSA can easily bend and affect the radiation pattern. To overcome this, the substrate was extended sideways and two metallic clamps were added. After some simulations, the substrate width and the dimensions of the clamps were chosen to minimize its effect on the TSA performance. The total width of the substrate was selected to be 20 mm so that the antenna width is the same as a WR-10 flange. All the comparisons between simulations and measurements presented in the following sections include the effects of the metallic clamps.

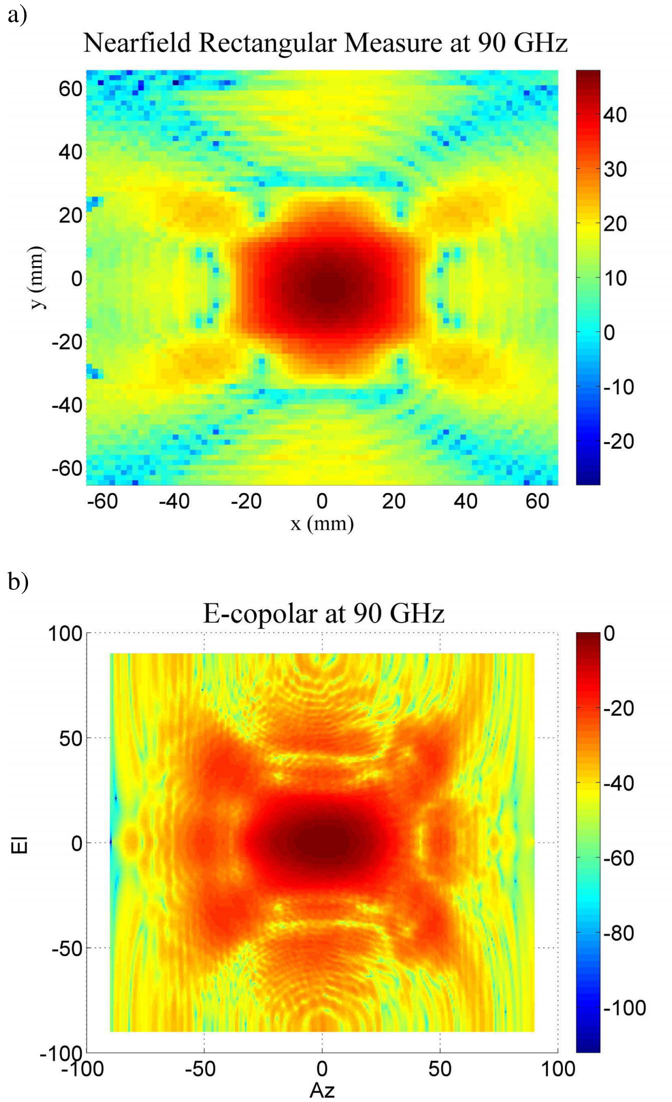

Fig. 8. Example of the characterization of the TSA. (a) Near-field copolar measurement. (b) Far-field transformed radiation pattern at 90 GHz.

III. Construction and Measurements

The TSA and its transition to the output waveguide were constructed using a Protolaser S from Laser & Electronics Company (LPKF) over Duroid 5880. First, they were etched over different sides of the same substrate. Then, the resulting circuit was placed in an aluminum split block containing the clamps for holding the antenna, and a groove and a cavity to place and align the transition. The block also contains the output waveguide. Fig. 6 shows the resulting construction.

Measured and simulated reflections, including the waveguide to microstrip transition, are shown in Fig. 7. Reflections are below -12 dB in the complete W-band. In the first part of the W-band, a good agreement with simulations is obtained. The discrepancy above 101 GHz is attributed to construction problems in the waveguide-to-microstrip transition not being fully aligned in the waveguide. It has to be noted that below 75 GHz, reflections increase because the transitions were designed to operate only above this frequency.

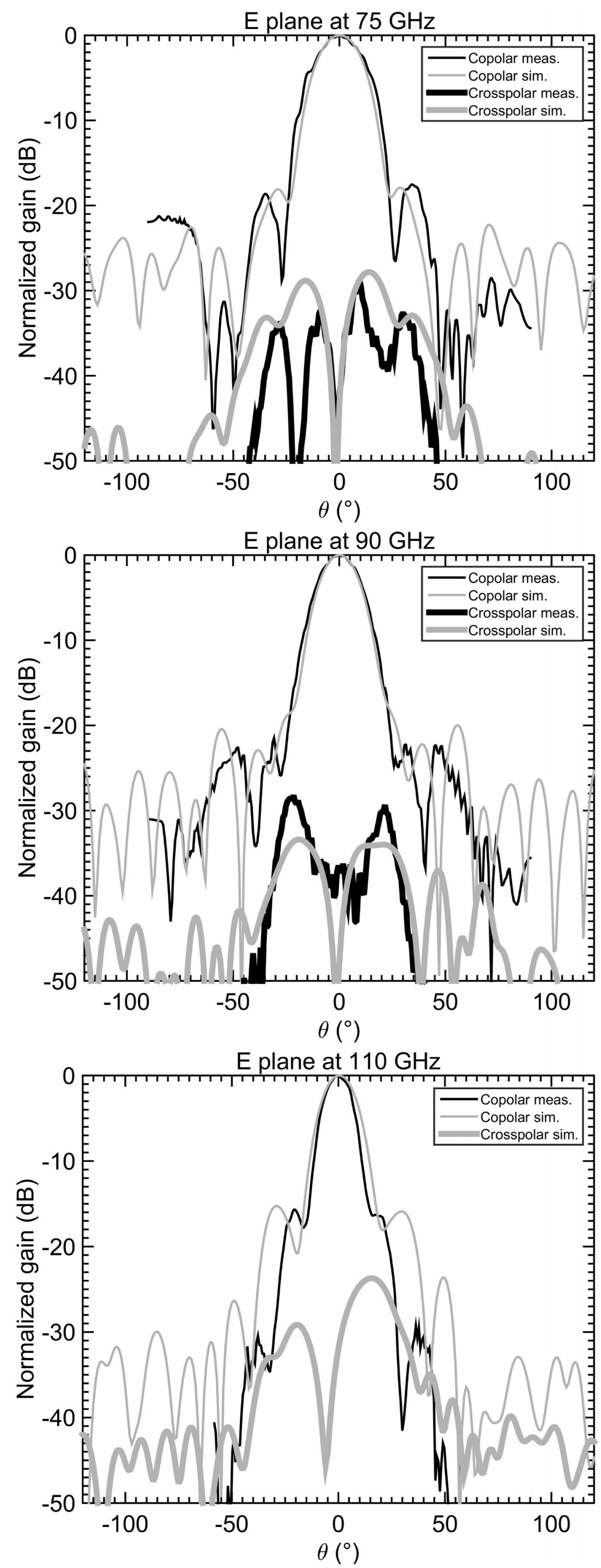

Fig. 9. E-plane radiation patterns at 75, 90, and 110 GHz. Measured copolar (black thin line) and cross polar (black thick line), and simulated copolar (gray thin line) and cross polar (gray thick line).

To characterize the antenna, a near-field pattern setup covering the frequency range from 75–110 GHz was constructed. An open-ended waveguide was selected as probe antenna.

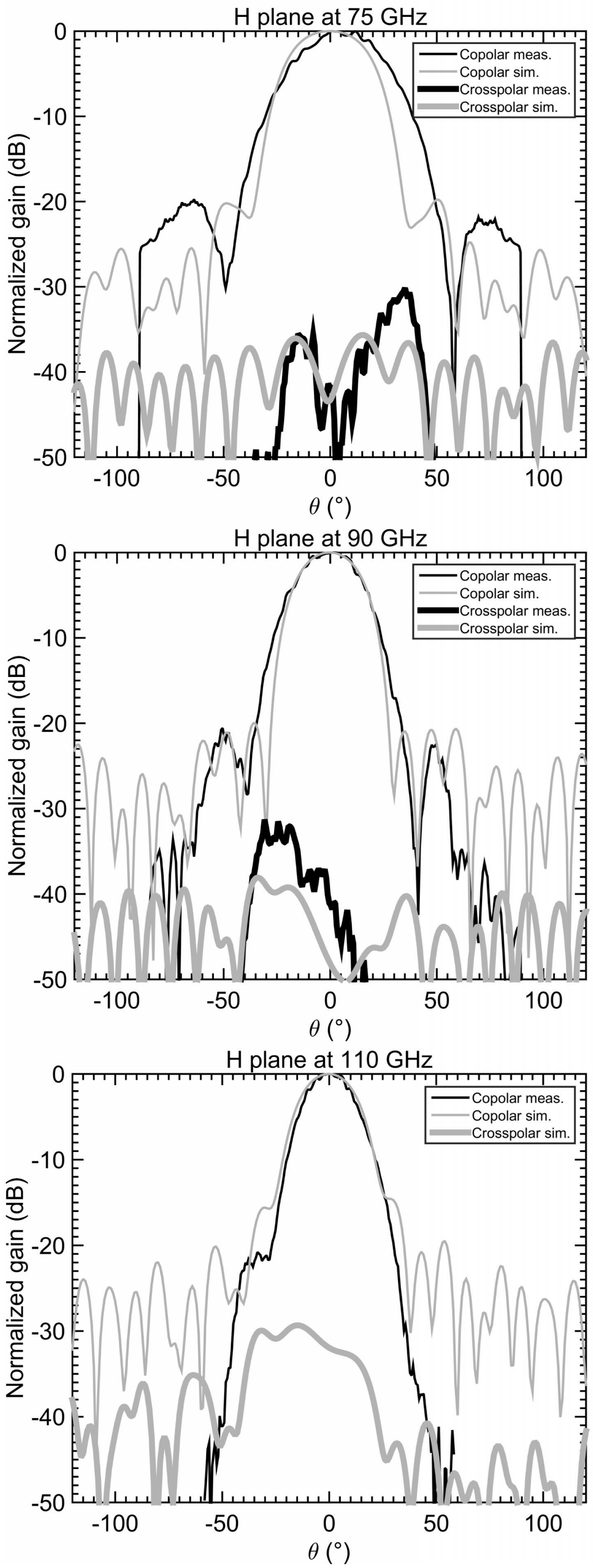

Fig. 10. H-plane radiation patterns at 75, 90, and 110 GHz. Measured copolar (black thin line) and cross polar (black thick line), and simulated copolar (gray thin line) and cross polar (gray thick line).

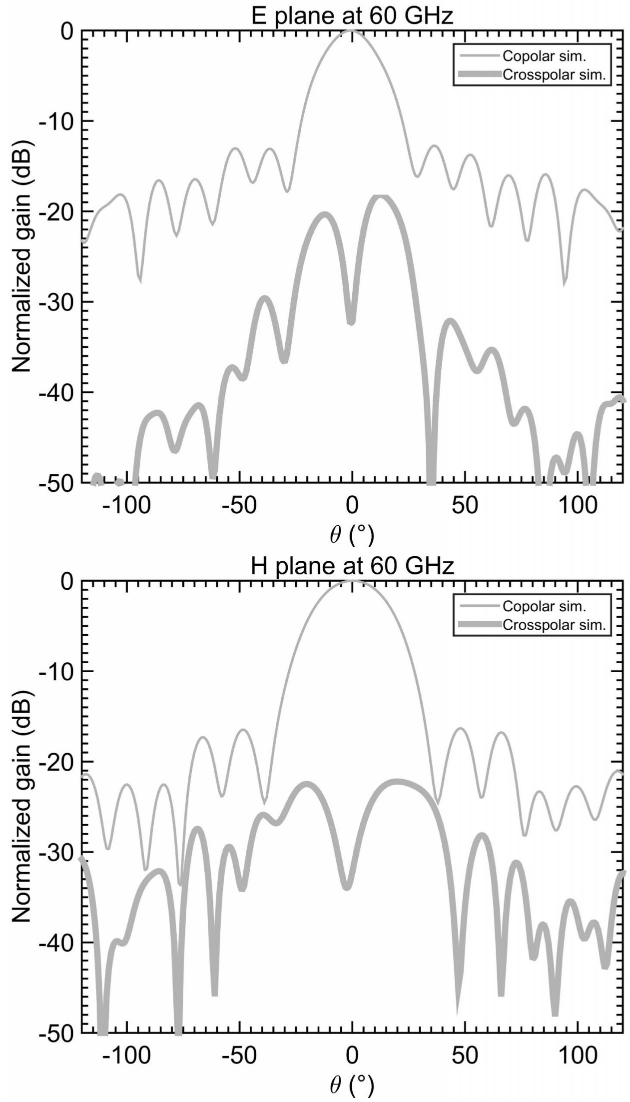

Fig. 11. Simulated copolar (gray thin line) and cross polar (gray thick line) radiation patterns at 60 GHz.

The distance between the TSA and the probe was larger than $3\lambda_0$ at 75 GHz, to be outside the reactive region. For each frequency, a sampling factor of $0.48\lambda_0$ was used to scan the near-field and avoid aliasing. To have a proper measurement of the antenna sidelobes, a half-angle of 60° was selected to define the scanning area. The near-field measurement is transformed to the far-field using a custom-made algorithm. Before measuring the TSA, the near-field setup and far-field transformation were tested using a standard pyramidal horn. The measurements were in excellent agreement with HFSS simulations.

Fig. 8 presents the near-field measurement and the transformed far-field radiation pattern of the TSA at 90 GHz. According to the coordinate axes defined in Fig. 1, the E- and H-planes are obtained by varying θ at $\phi = \pi/2$ and $\phi = 0$, respectively. Figs. 9 and 10 show the measured and simulated E- and H-planes at different frequencies. The far-field pattern agrees very well with simulations. At 90 GHz, the E- and H-planes beamwidths are 19° and 29°, respectively, as expected. Sidelobes are below -19 dB at the beginning and middle part of the band but increase slightly to -16 dB at 110 GHz. Cross-polarization measurements at 75 and 90 GHz are below -26 dB for $\phi = \pm\pi/4$ with varying θ. At 110 GHz, the cross polarization could not be measured but the simulation predicted values below −25 dB. The H-plane is not completely symmetrical, probably due to an alignment problem in the anechoic chamber. In fact, it can be seen in Fig. 8 that the beam is not completely centered.

Finally, Fig. 11 presents simulations performed to test the performance of the antenna at 60 GHz. They still predict a reasonable performance (sidelobes and cross polarization at −14 and −18 dB, respectively) despite the fact that the antenna was not optimized below 75 GHz. Further optimization promises ultrabroadband operation with excellent properties.

IV. Conclusion

An mm-wave TSA has been presented. Using PSO and an adaptable design for the TSA, it has been possible to enhance its radiation properties enabling its use in demanding applications, such as radio astronomy or telecommunications, as active antennas. By adding optimizable corrugations and a 10-segment profile, a VSWR < 1.6 and sidelobes below −16 dB were obtained. Far-field copolar and cross-polar measurements are in good agreement with simulations performed in HFSS. The optimized corrugated TSA presented here is suitable for use in applications where small antenna separations are required such as in mm-wave imaging or focal-plane arrays.

Acknowledgment

The authors would like to thank J. Pizarro for his work in the mechanical workshop and M. Adams for reviewing this paper. C. Jarufe would also like to thank CONICYT-PCHA/DoctoradoNacional/2013-21130609.

References

[1] P. Gibson, "The vivaldi aerial," in *Proc. 9th Eur. Microw. Conf.*, Sep. 1979, pp. 101–105.

[2] D. Schaubert, E. Kollberg, T. Korzeniowski, T. Thungren, J. Johansson, and K. Yngvesson, "Endfire tapered slot antennas on dielectric substrates," *IEEE Trans. Antennas Propag.*, vol. AP-33, no. 12, pp. 1392–1400, Dec. 1985.

[3] D. S. Woo, K. W. Kim, and H.-C. Choi, "A broadband and high gain tapered slot antenna for W-band imaging array applications," *Int. J. Antennas Propag.*, vol. 2014, Nov. 2014, Art. no. 378527.

[4] K. S. Yngvesson, T. L. Korzeniowski, Y.-S. Kim, E. L. Kollberg, and J. F. Johansson, "The tapered slot antenna—A new integrated element for millimeter-wave applications," *IEEE Trans. Microw. Theory Techn.*, vol. 37, no. 2, pp. 365–374, Feb. 1989.

[5] G. W. Kant, P. D. Patel, S. J. Wijnholds, M. Ruiter, and E. van der Wal, "EMBRACE: A multi-beam 20,000-element radio astronomical phased array antenna demonstrator," *IEEE Trans. Antennas Propag.*, vol. 59, no. 6, pp. 1990–2003, Jun. 2011.

[6] N. Jastram and D. S. Filipović, "Wideband millimeter-wave surface micromachined tapered slot antenna," *IEEE Antennas Wireless Propag. Lett.*, vol. 13, pp. 285–288, 2014.

[7] A. Rebollo, R. Gonzalo, and I. Ederra, "Full W-band microstrip fed vivaldi antenna," *J. Infr., Millim., Terahertz Waves*, vol. 37, no. 8, pp. 786–794, 2016.

[8] C. Rusch, J. Schäfer, T. Kleiny, S. Beer, and T. Zwick, "W-band vivaldi antenna in LTCC for CW-radar nearfield distance measurements," in *Proc. 5th Eur. Conf. Antennas Propag. (EUCAP)*, Apr. 2011, pp. 2124–2128.

[9] H. Ansoft, "Ver. 13," Ansoft Corp., Pittsburgh, PA, USA, Tech. Rep., 2011.

[10] S. Sugawara, Y. Maita, K. Adachi, K. Mori, and K. Mizuno, "Characteristics of a MM-wave tapered slot antenna with corrugated edges," in *IEEE MTT-S Int. Microw. Symp. Dig.*, vol. 2. Jun. 1998, pp. 533–536.

[11] A. R. Jordehi and J. Jasni, "Parameter selection in particle swarm optimisation: A survey," *J. Experim. Theor. Artif. Intell.*, vol. 25, no. 4, pp. 527–542, 2013.

[12] J. Robinson and Y. Rahmat-Samii, "Particle swarm optimization in electromagnetics," *IEEE Trans. Antennas Propag.*, vol. 52, no. 2, pp. 397–407, Feb. 2004.

[13] J. Kennedy and W. M. Spears, "Matching algorithms to problems: An experimental test of the particle swarm and some genetic algorithms on the multimodal problem generator," in *Proc. IEEE Int. Conf. Evol. Comput., IEEE World Congr. Comput. Intell.*, May 1998, pp. 78–83.

[14] S. Sugawara, Y. Maita, K. Adachi, K. Mori, and K. Mizuno, "A mm-wave tapered slot antenna with improved radiation pattern," in *IEEE MTT-S Int. Microw. Symp. Dig.*, vol. 2, Jun. 1997, pp. 959–962.

[15] R. E. Collin, *Antennas and Radiowave Propagation*. New York, NY, USA: McGraw-Hill, 1985.

[16] R.-Y. Fang and C.-L. Wang, "Wideband slotline-to-rectangular waveguide transition using truncated bow-tie antenna," in *Proc. Asia–Pacific Microw. Conf. (APMC)*, Dec. 2006, pp. 1395–1398.

[17] B. Shuppert, "Microstrip/slotline transitions: Modeling and experimental investigation," *IEEE Trans. Microw. Theory Techn.*, vol. MTT-36, no. 8, pp. 1272–1282, Aug. 1988.

[18] J. Kooi, G. Chattopadhyay, F. Rice, J. Zmuidzinas, S. Withington, and G. Yassin, "A full-height waveguide to thinfilm microstrip transition," in *Proc. 9th Int. Conf. Therahertz Electron.*, 2001, pp. 15–16.

Claudio Jarufe received the Degree in electrical engineering and the M.S. degree in physics from the Universidad de Chile, Santiago, Chile, in 2011 and 2012, respectively, where he is currently pursuing the Ph.D. degree in electrical engineering, with a focus on the development of millimeter-wave electronics for radio astronomy receivers.

In 2013, he was an intern with the Yebes Observatory, Guadalajara, Spain, where he was involved in developing low-noise amplifiers at Q-band. His current research interests include cryogenic low-noise amplifiers and receivers, microwave integrated circuits, microwave mixers, wideband antennas, and compact heterodyne cameras.

Rafael Rodriguez received the Degree and Ph.D. degree in electric engineering, with a focus on radio astronomy instrumentation with the Southern Millimeter Wave Telescope, a radio telescope based with the Astronomy Department, from the University of Chile, Santiago, Chile, in 2008 and 2015, respectively.

He was in charge of the upgrading of the front end with the Astronomy Department, Universidad de Chile, where he was a Post-Doctoral Researcher with the Millimeter Wave Laboratory, from 2015 to 2017. He is currently a Post-Doctoral Researcher with the Astronomy Department, Universidad de Chile.

Valeria Tapia received the Degree and M.Sc. degree (with maximum distinction) in electrical engineering from the Universidad de Chile, Santiago, Chile, in 2015.

She was involved in researching optical systems for heterodyne receivers at GHz frequencies and in the development of a refractive optical system at 35–52 GHz and 67–116 GHz for the Atacama Large Millimeter/Submillimeter Array (ALMA), the largest current observatory. She has completed several internships. During her master's degree, she visited the Advanced Technology Center, NAOJ, Japan, where she was involved in the improvement of ALMA Band 1 optical system. She joined the ALMA OSF, Atacama Chilean desert, to design and test CAN bus controlled prototypes to the Correlator and DST Laboratory. Moreover, she has participated three times in optical characterization campaigns in the European Southern Observatory, Germany. Her current research interests include radio astronomy instrumentation, microwave and millimeter-wave systems, and high-frequency communications.

Pablo Astudillo received the B.Sc. degree in electrical engineering and the master's degree in electrical civil engineering from the Universidad de Chile, Santiago, Chile.

In 2013, he joined the Radio Astronomical Instrumentation Group at Universidad de Chile, where he was involved in the design and construction of RF systems for antenna characterization. Since 2016, he has been involved in the operation, maintenance, and upgrade of the 1.2 m Southern Millimeter Wave Telescope. He is currently with the Cerro Calan National Astronomical Observatory, Santiago, Chile.

David Monasterio received the B.S. degree in electrical engineering and the master's degree in electrical civil engineering from the Universidad de Chile, Santiago, Chile, in 2010 and 2013, respectively.

Since 2013, he has been with the Millimeter/Submillimeter Wave Laboratory, Universidad de Chile. His current research interests include radio astronomy instrumentation, planar antennas, phased array, local oscillators, antenna beam pattern measurements, passive microwave components, microwave mixers, and monolithic microwave integrated circuit.

Rocio Molina received the B.Sc. and M.Sc degreesin electrical engineering, with a focus on antennas and optics designs including the optics for heterodyne cameras in millimeter-waves, from the Universidad de Chile, Santiago, Chile, in 2015 and 2017, respectively. .

Since 2014, she has been an Active Member of the Millimeter Wave Laboratory, Astronomy Department, Universidad de Chile.

F. P. Mena received the B.S. degree in physics from the Escuela Politcnica Nacional, Quito, Ecuador, in 1994, and the M.S. and Ph.D. degrees in physics from the University of Groningen, Groningen, The Netherlands, in 2000 and 2004, respectively.

In 2004, he joined the Low Energy Division, The Netherlands Institute for Space Research, Groningen, as an Instrument Scientist. In 2008, he was with the Universidad de Chile, Santiago, Chile, where he Co-Founded the Radio Astronomical Instrumentation Group and the Millimeter/Submillimeter Wave Laboratory. He is currently an Associate Professor with the Electrical Engineering Department, Universidad de Chile.

Nicolas Reyes received the Ph.D. degree in electrical engineering from the Universidad de Chile, Santiago, Chile, in 2013.

In 2013, he joined the Max Planck Institute for Radio Astronomy, Bonn, Germany, as a Post-Doctoral Researcher for the SOFIA project, where he was involved in terahertz instrumentation and multipixel receivers. In 2015, he was with the Millimeter/Submillimeter Wave Laboratory, Universidad de Chile. He is currently an Assistant Professor with the Electrical Engineering Department, Universidad de Chile. His current research interests include low-noise electronic, antennas, numerical simulation, and radio astronomy instrumentation.

Leonardo Bronfman received the M.Sc. in physics from the Universidad de Chile, Santiago, Chile, in 1980, and the Ph.D. degree in astrophysics from Columbia University, New York, NY, USA, in 1986, with the first complete CO Survey of the southern Milky Way.

He has been a Full Professor with the Department of Astronomy, Universidad de Chile since 1998, where he was the Department Chairman from 1993 to 1996 and from 2005 to 2008. He was an Associate Researcher with the European Southern Observatory (ESO) from 1990 to 1991, a Visiting Scientist with National Astronomical Observatory of Japan, Tokyo, Japan, in 1996, and a Visiting Scientist with National Radio Astronomy Observatory, Charlottesville, VA, USA, in 1998. Since 2008, he has been a Principal Investigator for Astronomical Instrumentation with the Universidad de Chile Center of Excellence for Astrophysics and Related Technologies, where he was involved in the implementation of the Millimeter Wave Laboratory, Cerro Calan National Astronomical Observatory. The Universidad de Chile's Millimeter Wave Laboratory has developed a prototype receiver for Atacama Large Millimeter/Submillimeter Array (ALMA) Band 1, and currently producing the optics for the full ALMA Band 1 receiver suit. His current research interests include galactic ISM, massive star formation, and mm-wave instrumentation.